Journal of the Brazilian Society of Mechanical Sciences and Engineering (2021) 43:384
https://doi.org/10.1007/s40430-021-03084-4

TECHNICAL PAPER

A simplified $k-\epsilon$ turbulence model

Darci Luiz Savicki[1] · **Antonio Goulart**[1] · **Gabriel Zardo Becker**[1]

Received: 9 March 2020 / Accepted: 28 May 2021 / Published online: 12 July 2021

Abstract
In this paper, we present a modification in the standard $k-\epsilon$ turbulence model, together with a new equation to express μ_t as a function of k and ϵ. In this simplified model, new values of the constants $c_{\epsilon 1}$, $c_{\epsilon 2}$ and σ_ϵ are provided. Using this model, we find an algebraic equation to express the viscosity in the wall (μ_w) so that the flow remains unchanged throughout the domain. Fitting the numerical solution, we find algebraic equations to approximate the k and ϵ profiles. Using periodic boundary conditions to solve k and ϵ equations, this model was applied to simulate the pollutant dispersion for the unstable Praire Grass experiments, obtaining a good agreement with the experimental data.

Keywords Unstable Boundary Layer · Turbulence Models · Pollutant Dispersion

1 Introduction

The $k-\epsilon$ turbulence model is routinely used by wind engineers and researchers to model the Atmospheric Boundary Layer (ABL). Despite the great advances already achieved, there are many challenges to be overcome.

For example, Mazzoldi, Hill and Colls [9], when using the standard $k-\epsilon$ model, simulated diffusion at stable, neutral and unstable atmospheric conditions, comparing it with Prairie Grass and Kit Fox experiments. They obtained an overestimation of concentrations distant from the source under unstable conditions, which is believed to be due to the underestimation of the turbulent dissipation of the turbulence model. Pontiggia et al. [14] also using the standard $k-\epsilon$ model concluded that the model tends to overestimate both the turbulence and the concentrations.

Richards and Hoxey [16] recommended modeling the atmospheric surface layer as a horizontally homogeneous turbulent boundary layer (HHTBL), where properties are considered constant in the horizontal direction and can vary only in the vertical direction. Under such conditions, they provided an analytic solution for the $k-\epsilon$ turbulence model, showing that the required horizontal homogeneity is satisfied. These profiles have been widely used as inlet boundary conditions for many types of turbulent flows.

On the other hand, Hargreaves and Wright [7] showed that, even setting appropriate turbulence profiles, the values of k and ϵ will not be maintained along the flow, as often is assumed. Contrariwise, turbulence profiles decay along the flow. They recommended using a modified law of the wall with a shear stress applied to the top boundary of the domain to get this homogeneity.

In [10], the authors argue that problems with excessive generation of turbulence close to the ground can be found when modeling the atmospheric surface layer as a HHTBL. Also, in [11], the authors show that when profiles intended for a shear driven situation are used, but without the driving shear stress, it leads to significant changes as the flow relaxes toward matching the free slip boundary condition at the top of the domain.

In this paper, we intend to contribute toward the solution of this problem, providing some modifications on the standard $k-\epsilon$ model, along with a new equation to express μ_t as function of k and ϵ, as well as new values for their constants, together with analytic profiles to k and ϵ. In addition, a new way to express the wall viscosity is presented. It was verified that these formulations are more robust and stable than the standard $k-\epsilon$ model and provide physically realistic results.

Technical Editor: Daniel Onofre de Almeida Cruz.

✉ Darci Luiz Savicki
darcisavicki@furg.br

Antonio Goulart
antonio.goulart@gmail.com

[1] Institute of Mathematics, Statistics and Physics, FURG, Rio Grande, RS, Brazil- Campus Carreiros: Av. Itália km 8 Bairro Carreiros, Rio Grande, Brazil

2 Mathematical model

2.1 Atmospheric boundary layer

In the atmospheric boundary layer (ABL), turbulence is responsible for the vertical mixture of physical quantities, such as momentum, heat, moisture and pollutants, as an example. The height of the ABL is very important for atmospheric dispersion because it determines the volume available for diluting the pollutant.

During the day, the ABL is generally convective due to the warming of the Earth's surface (Convective Boudary Layer - CBL). At night, due to the cooling of Earth's surface, the ABL is usually stable (Stable Boundary Layer - SBL). Neutral boundary layers are rare and can only occur on days with strong surface winds and cloudy skies, for example.

The lowest part of the ABL is called the atmospheric surface layer (typically, 0.1 of the height of the ABL). In the surface layer, shear always exceeds buoyancy due to the strong surface drag.Above it, in the mixed layer, buoyancy is the main factor of convective turbulence.

2.2 Neutral horizontally homogeneous turbulent boundary layer

According to [16], the neutral atmospheric boundary layer in the steady state can be modeled as a horizontally homogeneous turbulent boundary layer (HHTBL). Using the the standard $k-\epsilon$ turbulence model, they modeled the HHTBL as

$$u = \frac{u_\star}{\kappa} ln\left(\frac{z+z_0}{z_0}\right) \tag{1}$$

$$0 = \frac{\partial}{\partial z}\left(\frac{\mu_t}{\sigma_k}\frac{\partial k}{\partial z}\right) + P_k - \rho\epsilon \tag{2}$$

$$0 = \frac{\partial}{\partial z}\left(\frac{\mu_t}{\sigma_\epsilon}\frac{\partial \epsilon}{\partial z}\right) + [c_{\epsilon 1}P_k - c_{\epsilon 2}\rho\epsilon]\frac{\epsilon}{k} \tag{3}$$

where P_k denotes the production of turbulent kinetic energy, defined as

$$P_k = \mu_t\left(\frac{du}{dz}\right)^2 \tag{4}$$

and $u_\star$ is the friction velocity, defined as

$$u_\star = \frac{\kappa u_r}{ln\left(\frac{h_r+z_0}{z_0}\right)} \tag{5}$$

that is calculated from previous information of velocity (u_r) at reference height (h_r). The soil surface roughness is represented by z_0.

The analytic solution of this system is

$$k = \frac{u_\star^2}{\sqrt{c_\mu}} \tag{6}$$

$$\epsilon = \frac{u_\star^3}{\kappa(z+z_0)} \tag{7}$$

where the turbulent eddy viscosity μ_t is expressed as

$$\mu_t = \rho c_\mu \frac{k^2}{\epsilon} \tag{8}$$

Using Eqs. (6, 7), equation (8) can be written as

$$\mu_t = \rho u_\star \kappa(z+z_0) = \rho\kappa c_\mu^{\frac{1}{4}} k^{\frac{1}{2}}(z+z_0) \tag{9}$$

It is easy to see that Eqs. (6, 7, 9) satisfies Eq. (2). On the other hand, to be consistent with Eq. (3) the constants of this equation must obey the relation

$$\kappa = \sqrt{(c_{\epsilon 2} - c_{\epsilon 1})\sigma_\epsilon\sqrt{c_\mu}} \tag{10}$$

As an example, for standard $k-\epsilon$ turbulence model, the constants $c_{\epsilon 1} = 1.44, c_{\epsilon 2} = 1.92, \sigma_\epsilon = 1.3; c_\mu = 0.09$ result in $\kappa = 0.432$, which is close to the normal value of the von Kármán constant ($\kappa = 0.41$).

For this model, the same solution can be find if the eddy viscosity is expressed as a linear function of k in the form

$$\mu_t = \rho c_\mu k^\star \frac{k}{\epsilon} \tag{11}$$

where $k^\star = k = \frac{u_\star^2}{\sqrt{c_\mu}}$.

So, we can ask if this linear relationship between k and μ_t is still valid, if μ_t is expressed in a simpler form, as in

$$\mu_t = \rho k^\star \frac{k}{\epsilon} \tag{12}$$

This question will be investigated in the following sections.

2.3 Unstable horizontally homogeneous turbulent toundary layer

The turbulent boundary layer is considered unstable when it supports vertical movement due to buoyancy. To model the turbulent boundary layer, let's include the buoyancy term G_k in the HHTBL model. Then, the standard $k-\epsilon$ model takes the form

$$0 = \frac{\partial}{\partial z}\left(\frac{\mu_t}{\sigma_k}\frac{\partial k}{\partial z}\right) + P_k + G_k - \rho\epsilon \tag{13}$$

$$0 = \frac{\partial}{\partial z}\left(\frac{\mu_t}{\sigma_\epsilon}\frac{\partial \epsilon}{\partial z}\right) + [c_{\epsilon 1}(P_k + c_{\epsilon 3}G_k) - c_{\epsilon 2}\rho\epsilon]\frac{\epsilon}{k} \tag{14}$$

where

$$G_k = -\mu_t g\beta\frac{\partial T}{\partial z} \tag{15}$$

For an unstable turbulent boundary layer, the velocity profile can be modeled as

$$u = \frac{u^*}{\kappa} ln\left(\frac{z + z_0}{z_0} + \psi_m\left(\frac{z}{L}\right)\right) \tag{16}$$

where ψ_m, for $\frac{1}{L} < 1$, is $\psi_m\left(\frac{z}{L}\right) = ln\left(\frac{1+x^2}{2}\right) + ln\left(\frac{1+x}{2}\right)^2 - 2tg^{-1}(x) + \frac{\pi}{2}$, with $x = (1 - 15\frac{z}{L})^{\frac{1}{4}}$, and L is the Monin-Obukhov length, defined as

$$L = \frac{u_\star^3\theta_0}{\kappa g\overline{w'\theta'_v}} \tag{17}$$

where θ_0 is the surface (virtual) potential temperature, $\overline{w'\theta'_v}$ is the kinematic vertical turbulent flux of virtual potential temperature near the surface, g is the gravity acceleration, and κ is the von Kármán constant.

In the next sections, we will make some changes to this model and then solve it using numerical simulation.

2.4 The Troen and Mahrt equation for μ_t

The Troen e Mahrt equation to eddy viscosity for unstable atmospheric stratification [18] is

$$\mu_t(z) = \rho\kappa w_s z\left(1 - \frac{z}{z_i}\right)^p \tag{18}$$

where $w_s = 0.65w_\star$ for $z_i >> -L$. The convective velocity scale $w_\star$ is defined as

$$w_\star = \left(\frac{g}{\theta_0} z_i \overline{w'\theta'_v}\right)^{\frac{1}{3}} \tag{19}$$

where z_i is the height of the convective layer.

In [18], the authors suggest to take p between 2 and 3. However, more recently, some researchers (for example, [3] and [13]) recommend considering Eq. (18) with $p = 1$ and $w_s = w_\star$, so that

$$\mu_t(z) = \rho\kappa w_\star z\left(1 - \frac{z}{z_i}\right) \tag{20}$$

The relation between $u_\star$ and $w_\star$ can be expressed as [6].

$$u_\star = w_\star\left(\frac{z_i}{\kappa|L|}\right)^{-\frac{1}{3}} \tag{21}$$

Equation (20) predicts that the turbulent eddy viscosity has a maximum point in the middle of the convective boundary layer ($z = z_i/2$).

2.5 Mathematical equation to ϵ profile

Based on the measurements of turbulent kinetic energy budget terms in the surface layer over flat terrain [1], one can find

$$\epsilon(z) = \frac{u_\star^3}{\kappa z}\varphi_\epsilon\left(\frac{z}{L}\right) \tag{22}$$

For negative Monin-Obukhov length ($L < 0$), $\varphi_\epsilon = 1 - (\frac{z}{L})$, so one can find

$$\epsilon(z) = \frac{u_\star^3}{\kappa z}\left(1 - \frac{z}{L}\right) = \frac{u_\star^3}{\kappa z} - \frac{u_\star^3}{\kappa z}\frac{z}{L} = \frac{u_\star^3}{\kappa z} + \epsilon_0 \tag{23}$$

where

$$\epsilon_0 = -\frac{u_\star^3}{\kappa L} \tag{24}$$

2.6 Mathematical equation for k profile

As showed by [5], in a convective atmosphere, the turbulent kinetic energy shows a parabolic profile in the vertical direction. So, let us express k in a similar way of Eq. (20), it is

$$k = \alpha z\left(1 - \frac{z}{z_i}\right) \tag{25}$$

where α is an undetermined parameter. Considering the profiles for k and ϵ (Eq. (25) and (23)), we can see that the usual equation

$$\mu_t = \rho c_\mu \frac{k^2}{\epsilon} \tag{26}$$

will result in a polynomial of degree greater than 2, that is inconsistent with Eq. (20) (taking $p = 1$). This inconsistency can be solved by taking the ratio $\frac{k}{\epsilon}$ (not $\frac{k^2}{\epsilon}$) in the equation for μ_t, as suggested in Eq. (12). Let us show this in more detail in the next section.

2.7 Mathematical equation for μ_t as function of the ratio $\frac{k}{\epsilon}$

First we consider the advection layer, where $z << -L$, so that $\epsilon = \frac{u_\star^3}{\kappa z} - \frac{u_\star^3}{\kappa L} \approx \frac{u_\star^3}{\kappa z}$.

Replacing equations (20), (25) and $\epsilon = \frac{u_\star^3}{\kappa z}$ in Eq. (12), we find

$$\rho w_\star \kappa z\left(1 - \frac{z}{z_i}\right) = \rho k^\star \frac{\alpha z\left(1 - \frac{z}{z_i}\right)}{\frac{u_\star^3}{\kappa z}} \tag{27}$$

Then solving Eq. (27) for α, results in

$$\alpha = \frac{w_\star u_\star^3}{k^\star z} \tag{28}$$

Moreover, when $z << z_i$, the flow is dominated by advective forces, so we can suppose $w_\star = u_\star$. In addition, to use the equation (12), let's assume that $k^\star = u_\star^2$. Then

$$\alpha = \frac{u_\star^2}{z} \tag{29}$$

Using Eq. (29), Eq. (25) can be expressed as

$$k = \alpha z \rightarrow k = u_\star^2 \tag{30}$$

Now, we consider the convective layer where $z >> -L$, so that $\epsilon = \frac{u_\star^3}{\kappa z} - \frac{u_\star^3}{\kappa L} \approx -\frac{u_\star^3}{\kappa L}$

Replacing equations (20), (25) and $\epsilon = -\frac{u_\star^3}{\kappa L}$ in Eq. (12), we find

$$\rho w_\star \kappa z\left(1 - \frac{z}{z_i}\right) = \rho k^\star \frac{\alpha z\left(1 - \frac{z}{z_i}\right)}{-\frac{u_\star^3}{\kappa L}} \tag{31}$$

Solving for α we find,

$$\alpha = -\frac{w_\star u_\star^3}{k^\star L}. \tag{32}$$

Then, by analogy with the previous results for the advective layer, we can propose $\alpha = \frac{\sqrt{w_\star u_\star^3}}{-L}$ (replacing z with $-L$ in Eq. (29) and $u_\star^2$ with $\sqrt{w_\star u_\star^3}$), so that $k^\star = \sqrt{w_\star u_\star^3}$.

Now, using Eq. (32), the turbulent kinetic energy (Eq. (25)), can be expressed as

$$k = \frac{\sqrt{w_\star u_\star^3}}{-L} z\left(1 - \frac{z}{z_i}\right) \tag{33}$$

In resume

$$if\ z << |-L| = \begin{cases} k = u_\star^2; k^\star = u_\star^2 \\ \epsilon \approx \frac{u_\star^3}{\kappa z} \\ \mu_t = \rho k^\star \frac{k}{\epsilon} = \rho u_\star \kappa z \end{cases} \tag{34}$$

$$if\ z >> |-L| = \begin{cases} k = \frac{\sqrt{w_\star u_\star^3}}{-L} z\left(1 - \frac{z}{z_i}\right); k^\star = \sqrt{w_\star u_\star^3} \\ \epsilon = -\frac{u_\star^3}{\kappa L} \\ \mu_t = \rho k^\star \frac{k}{\epsilon} = \rho w_\star \kappa z\left(1 - \frac{z}{z_i}\right) \end{cases} \tag{35}$$

Equations 34 and 35 show that the profile of μ_t varies from one polynomial $P_1(z)$ to $P_2(z)$ when the dominant forces vary from advection ($z >> z_i$) to convection ($z << z_i$), respectively. Moreover, the turbulent kinetic energy varies from ($P_0(z)$) to a $P_2(z)$ as long as the dominant forces vary from advection to convection.

3 The simplified $k - \epsilon$ turbulence model

The derivation of the $k - \epsilon$ equations is given in [4]. After a tedious manipulation, the equation of ϵ can be written as

$$\rho \frac{\partial \epsilon}{\partial t} + \rho U_j \frac{\partial \epsilon}{\partial x_j} = \frac{\partial}{\partial x_j}\left(\left(\mu + \frac{\mu_t}{\sigma_\epsilon}\right)\frac{\partial \epsilon}{\partial x_j}\right) + P_\epsilon + D_\epsilon \tag{36}$$

The first term on the right hand side (RHS) of Eq. (36) models the transport of dissipation due to viscous diffusion, turbulent fluctuations and pressure-velocity fluctuations. The second (P_ϵ) represents the production of dissipation due to interactions between the mean flow and the products of the turbulent fluctuations. The last term on the RHS (D_ϵ) represents the destruction rate of dissipation due to the turbulent velocity fluctuations.

The term P_ϵ can be regarded as a production of ϵ. To model this term, let us to consider the assumption of local equilibrium, namely $P_k \approx \epsilon$. Since, for local equilibrium, the rate at which k is produced is equal to ϵ, the only time scale (characteristic time scale) that can define the rate of change of ϵ must scale with k (or $k^\star$). This implies that

$$P_\epsilon \propto \frac{P_k}{t_{ch}} \tag{37}$$

Here, we define the characteristic time scale as

$$t_{ch} = \frac{k^\star}{\epsilon} \tag{38}$$

that results in

$$P_\epsilon \propto P_k \frac{\epsilon}{k^\star} \tag{39}$$

In a similar manner, the term D_ϵ can be taken to represent the time rate at which dissipation is dissipated. So, this can be thought of as being given by

$$D_\epsilon \propto \frac{\epsilon}{t_{ch}} \tag{40}$$

Using the characteristic time scale (Eq. (38)), results in

$$D_\epsilon \propto \epsilon \frac{\epsilon}{k^\star} \tag{41}$$

Collecting the modeled terms, Eq. (36) is given by

$$\rho \frac{\partial \epsilon}{\partial t} + \rho U_j \frac{\partial \epsilon}{\partial x_j} = \frac{\partial}{\partial x_j}\left(\left(\mu + \frac{\mu_t}{\sigma_\epsilon}\right)\frac{\partial \epsilon}{\partial x_j}\right) + c_{\epsilon 1} P_k \frac{\epsilon}{k^\star} - c_{\epsilon 2}\epsilon \frac{\epsilon}{k^\star} \tag{42}$$

Moreover, defining the characteristic length scale as

$$l_{ch} = k^{\frac{1}{2}} \frac{k^\star}{\epsilon} \tag{43}$$

the eddy viscosity is

$$\mu_t = \rho k^{\frac{1}{2}} l_{ch} = \rho k^{\frac{1}{2}}\left(k^{\frac{1}{2}} \frac{k^\star}{\epsilon}\right) = \rho k^\star \frac{k}{\epsilon} \tag{44}$$

In addition, the turbulent kinetic energy in the standard $k-\epsilon$ model is

$$\rho \frac{\partial k}{\partial t} + \rho U_j \frac{\partial k}{\partial x_j} = \frac{\partial}{\partial x_j}\left(\left(\mu + \frac{\mu_t}{\sigma_\epsilon}\right)\frac{\partial k}{\partial x_j}\right) + P_k - \rho \epsilon_s \tag{45}$$

Here, we are going to focus on just the term $-\rho\epsilon_s$ of the standard k-equation, where, for clarification, we will use the subscript s to emphasize the standard model. The variable ϵ_s is generally modeled as (see [4])

$$\epsilon_s = \frac{k^{3/2}}{l_{ch}} \tag{46}$$

Now, using the previous length scale definition ($l_{ch} = \frac{k^{1/2}k^\star}{\epsilon}$), (Eq. (43)), we can see that the ϵ_s is

$$\epsilon_s = \frac{k^{3/2}}{l_{ch}} = \frac{k^{3/2}}{\frac{k^{1/2}k^\star}{\epsilon}} = \epsilon \frac{k}{k^\star} \tag{47}$$

So, for our simplified $k-\epsilon$ mathematical model, the term "$-\rho\epsilon_s$" must be replaced by $-\rho\epsilon(\frac{k}{k^\star})$.

For more clarify, we repeat Eq. (42) and Eq. (45) (including the convective term G_k), to show the final form of the simplified $k-\epsilon$ turbulence equations, in two-dimensional form

$$\frac{\partial(\rho u k))}{\partial x} + \frac{\partial(\rho w k)}{\partial z} = \frac{\partial}{\partial x}\left[\left(\mu + \frac{\mu_t}{\sigma_k}\right)\frac{\partial k}{\partial x}\right] + \frac{\partial}{\partial z}\left[\left(\mu + \frac{\mu_t}{\sigma_k}\right)\frac{\partial k}{\partial z}\right] + P_k + G_k - \rho\epsilon\left(\frac{\mathbf{k}}{\mathbf{k}^\star}\right) \tag{48}$$

$$\frac{\partial(\rho u \epsilon))}{\partial x} + \frac{\partial(\rho w \epsilon)}{\partial z} = \frac{\partial}{\partial x}\left[\left(\mu + \frac{\mu_t}{\sigma_\epsilon}\right)\frac{\partial \epsilon}{\partial x}\right] + \frac{\partial}{\partial z}\left[\left(\mu + \frac{\mu_t}{\sigma_\epsilon}\right)\frac{\partial \epsilon}{\partial z}\right] c_{\epsilon 1} P_k \frac{\epsilon}{\mathbf{k}^\star} - \rho c_{\epsilon 2}\epsilon \frac{\epsilon}{\mathbf{k}^\star} \tag{49}$$

To get a physical meaning for $k^\star$, let's consider its value for the neutral atmosphere

$$k^\star = u_\star^2 \tag{50}$$

From the definition of friction velocity ($u_\star$), we have

$$u_\star = \sqrt{\frac{\tau_0}{\rho}} \tag{51}$$

Then, $k^\star$ can be read as

$$k^\star = u_\star^2 = \frac{\tau_0}{\rho} \tag{52}$$

In the inertial sublayer, the eddies can be considered isotropic, no longer having a memory of the shape of the large and highly anisotropic eddies. Thus, the presence of $k^\star$ in the $k-\epsilon$ equations as well as in the turbulent viscosity acts as a memory of the magnitude of the wall shear stress (τ_0).

For an unstable atmosphere, interpretation can be done in a similar way. For this case, we shows that $k^\star = \sqrt{{u_\star}^3 w_\star}$. Then $k^\star$ couples the effect of wall shear stress and buoyancy, represented by the friction and convection velocities, respectively.

3.1 Consistency of the simplified $k-\epsilon$ model for horizontally homogeneous turbulent boundary layer

For the HHTBL, our simplified $k-\epsilon$ model takes the form of

$$0 = \frac{d}{dz}\left(\frac{\mu_t}{\sigma_k}\frac{dk}{dz}\right) + \mu_t\left(\frac{du}{dz}\right)^2 - \rho\epsilon\frac{k}{k^\star} \tag{53}$$

$$0 = \frac{d}{dz}\left(\frac{\mu_t}{\sigma_\epsilon}\frac{d\epsilon}{dz}\right) + c_{\epsilon 1}\mu_t\left(\frac{du}{dz}\right)^2 \frac{\epsilon}{k^\star} - \rho c_{\epsilon 2}\epsilon\frac{\epsilon}{k^\star} \tag{54}$$

This mathematical model differs from equations (2, 3) in the manner of calculating μ_t, that is, while the standard model uses Eq. (8), the simplified model uses Eq. (12).

In section 2.7, we show that, for advection-dominated flow, we have $k^\star = {u_\star}^2, k = u_\star^2, \epsilon = \frac{u_\star^3}{\kappa z'} u = \frac{u_\star}{\kappa} ln(\frac{z'}{z_0})$ (so, $\frac{du}{dz} = \frac{u_\star}{\kappa z'}$), and $\mu_t = \rho k^\star \frac{k}{\epsilon} = \rho \kappa u_\star z'$. Here, for simplicity's sake, we define $z' = z + z_0$.

It is easy to see that Eq. (53) is immediately satisfied, as indicated below

$$0 = \frac{\partial}{\partial z}\left(\frac{\mu_t}{\sigma_k}0\right) + \rho\kappa u_\star z'\left(\frac{u_\star}{\kappa z'}\right)^2 - \rho\frac{{u_\star}^3}{\kappa z'}\frac{{u_\star}^2}{{u_\star}^2} \rightarrow 0 = 0 \tag{55}$$

On the other hand, for Eq. (54), we have

$$\frac{d}{dz}\left(\frac{\rho u_\star \kappa z'}{\sigma_\epsilon}\frac{d(\frac{u_\star^3}{\kappa z'})}{dz}\right) + c_{\epsilon 1}\rho\kappa u_\star z'\left(\frac{u_\star}{\kappa z'}\right)^2\frac{u_\star^3}{\kappa z'}\frac{1}{u_\star^2} - c_{\epsilon 2}\rho\frac{u_\star^3}{\kappa z'}\frac{u_\star^3}{\kappa z'}\frac{1}{u_\star^2} = 0 \tag{56}$$

After some algebra, we can find

$$\frac{1}{\sigma_\epsilon} + \frac{c_{\epsilon 1}}{\kappa^2} - \frac{c_{\epsilon 2}}{\kappa^2} = 0 \tag{57}$$

There are infinite combinations of values that satisfy this equation. For example, using $\sigma_\epsilon = 1.00, c_{\epsilon 1} = 1.00 - \delta, c_{\epsilon 2} = 1.00 + \delta, \kappa = 0.40$ we find $\sigma = 0.08$, so that, $c_{\epsilon 1} = 0.92, c_{\epsilon 2} = 1.08$. If we choose $c_{\epsilon 1} = 1.00$, then $c_{\epsilon 2} = 1.16$. And, if we choose $c_{\epsilon 2} = 1.00$, then $c_{\epsilon 1} = 0.84$. In sect. 5, we analyse the effect of these choices on the numerical solution. We can say that the effect is negligible in this range. So, by symmetry, let's adopt $c_{\epsilon 1} = 0.92$, $c_{\epsilon 2} = 1.08$ for our model.

In [15], data obtained from the direct numerical simulation (DNS) of the temporal mixture layer is presented, showing that $0.01 \lessapprox \mu_t \frac{\epsilon}{k^2} \lessapprox 0.017$.

Moreover, $\mu_t \frac{\epsilon}{k^2}$ is close to 0.09 everywhere except near the boundaries of the flows. This result agrees with the value $c_\mu = 0.09$ present in the standard $k - \epsilon$ turbulence model. So, applying this result to the simplified $k - \epsilon$ model (Eq. (12) , $\rho = 1$), we have

$$1 = \frac{\mu_t \epsilon}{k^\star k} = \frac{\mu_t \epsilon}{k^\star k}\frac{k}{k} = \left(\frac{\mu_t \epsilon}{k^2}\right)\frac{k}{k^\star} \tag{58}$$

From Eq. (58), we can extract that $\frac{k^\star}{k} = \mu_t \frac{\epsilon}{k^2}$. Let's consider $\alpha = \mu_t \frac{\epsilon}{k^2}$, then $\frac{k^\star}{k} = \alpha$, or $k^\star = \alpha k$, with $0.01 \leq \alpha \leq 0.017$. This equation shows that k changes in the inverse form of α, because $k^\star$ is constant. It should be noted that, although for HHTBL we find $k^\star = k = {u_\star}^2$, in general flows, $k^\star \neq k$.

3.2 Mathematical equation for $k^\star$

The main parameter of our simplified $k - \epsilon$ turbulence model is $k^\star$. In the previous section, we found that, for the advective layer, $k^\star$ can be expressed in the form of

$$k^\star = u_\star^2 \tag{59}$$

Also, for the convection layer, we show that $k^\star$ can be expressed in the form of

$$k^\star = \sqrt{w_\star {u_\star}^3} \tag{60}$$

In addition, we can represent $k^\star$ using the well-known inlet boundary condition for k , so that

$$k^\star = \frac{3}{2}(I u_{ref})^2 \tag{61}$$

where I is the turbulent intensity, and u_{ref} is the mean velocity at reference position.

In this work, we find a good agreement between inlet and outlet velocity profiles and between numerical and experiment concentrations (for the Praire-Grass experiments) using Eq. (59) for $k^\star$.

3.3 Developing a mathematical equation for μ_t at the wall

For the atmospheric boundary layer, it is desirable that the numerical simulation maintains the inlet velocity profile along the flow direction. In this sense, many researchers (for example, [8]) have proposed modifications to the standard $k - \epsilon$ model, as well as, to the viscosity at the wall.

It is important to note that the agreement between the inlet and outlet velocity profiles depends on the appropriate value of μ_w as well as the proper discretization of the term P_k, in particular, the derivative $\frac{du}{dz}$, due to the high gradient close to the ground.

We used one expression presented in [17], where $u'_k = \frac{du}{dz}$ are weighted average of $u'_{k-\frac{1}{2}}$ and $u'_{k+\frac{1}{2}}$, in the form

$$u'_k = \frac{h_k}{h_k + h_{k-1}}u'_{k-\frac{1}{2}} + \frac{h_{k-1}}{h_k + h_{k-1}}u'_{k+\frac{1}{2}} \tag{62}$$

where $u'_{k-\frac{1}{2}} = \frac{u_k - u_{k-1}}{z_k - z_{k-1}}$, $u'_{k+\frac{1}{2}} = \frac{u_{k+1} - u_k}{z_{k+1} - z_k}$, $h_{k-1} = z_k - z_{k-1}$ and $h_k = z_{k+1} - z_k$. The coefficients of $u'_{k-\frac{1}{2}}$ and $u'_{k+\frac{1}{2}}$ reflect the relative distances of the point k to the positions $k - \frac{1}{2}$ and $k + \frac{1}{2}$, with the greater weighting factor associated with the closest point.

In this work, the effect of the viscosity at the wall (μ_w) on the velocity profile was investigated. We find that the outlet velocity profile agrees with the inlet profile if the viscosity in the wall is higher than prescribed by the standard law of the wall. The appropriate value of μ_w was found by an iterative process in which, for the first volume in the vertical direction, the outlet velocity $u(z_2)_{out}$ must be close to the inlet velocity $u(z_2)_{in}$.

This value was calculated by the algorithm shown in Eqs. (63) and (64). By this algorithm, during the numerical simulation, we increase or decrease the value of μ_w depending on the difference between the inlet and outlet velocity in the position z_2, that is, in the first inner point.

$$f_{\mu,new} = \begin{cases} 1.01 f_\mu, & \text{if } u(z_2)_{out} > 1.1 u(z_2)_{in} \\ 0.99 f_\mu, & \text{if } u(z_2)_{out} < 0.9 u(z_2)_{in} \end{cases} \quad (63)$$

$$\mu_{w,new} = f_\mu [\rho \sqrt{k^\star}(z_2 + z_0)] \quad (64)$$

This procedure was applied to all nineteen unstable Praire-Grass experiments (see Table 2), with six different mesh refinement factors, as shown in Table 1. The number of volumes in the vertical direction is calculated by $M = Rz_i(\frac{500}{1340})$. The constant $\frac{500}{1340}$ refers to experiment number 7 ($z_i = 1340m$), where we found that $M = 500$ provides a good resolution. For the vertical direction, we use a non-uniform mesh, with more refinement at the bottom and in the axial direction, the mesh is more refined at the inlet of the flow, due to the discharge source.

Using the final values of f_μ and μ_w for each experiment as well as the mesh refinement, we construct the graphs shown in Fig. 1a.

Table 1 Mesh refinement used to adjust μ_w. $\left(M = Rz_i\left(\frac{500}{1340}\right)\right)$

Mesh number	f_M
1	0.25
2	0.5
3	0.75
4	1.0
5	1.5
6	2.0

Fitting the coefficient f_μ using the logarithmic model, we found

$$f_\mu = -0.07372 ln(z_2) - 0.09495 \quad (65)$$

Then, the wall viscosity can be expressed now by an algebraic equation, that is

$$\mu_{w,new} = (-0.07372 ln(z_2) - 0.09495)[\rho \sqrt{k^\star}(z_2 + z_0)] \quad (66)$$

It is important to emphasize that Eq. (66) uses the position z_2 to calculate μ_w, thus, it takes into account the mesh refinement.

In Fig. 1b, we show that the values of μ_w calculated using Eq. (64) agree very well with the values obtained from a numerical simulation. It is important to emphasize that this value of μ_w has been found to ensure that the inlet velocity profile remains unchanged throughout the flow, so that the inlet and outlet velocity profiles are in agreement.

Moreover, we found that there is a good correlation between μ_w and μ_2 (μ_2 is μ_t calculated at the first inner point in the outlet boundary), as shown in Fig. 2. This correlation is well adjusted by the equation $\mu_w = 0.21576 \mu_t(z_2)^{0.82097}$, where $\mu_t(z_2)$ is the turbulent viscosity at the first inner point z_2.

It is interesting that Eq. (64), is similar to that provided by [10], that is $\mu_t = \rho c_\mu^{\frac{1}{4}} \kappa k^{\frac{1}{2}} z$.

3.4 Overview of the simplified $k - \epsilon$ model

For clarity purposes, let us to enumerate the major modifications proposed in our simplified $k - \epsilon$ model

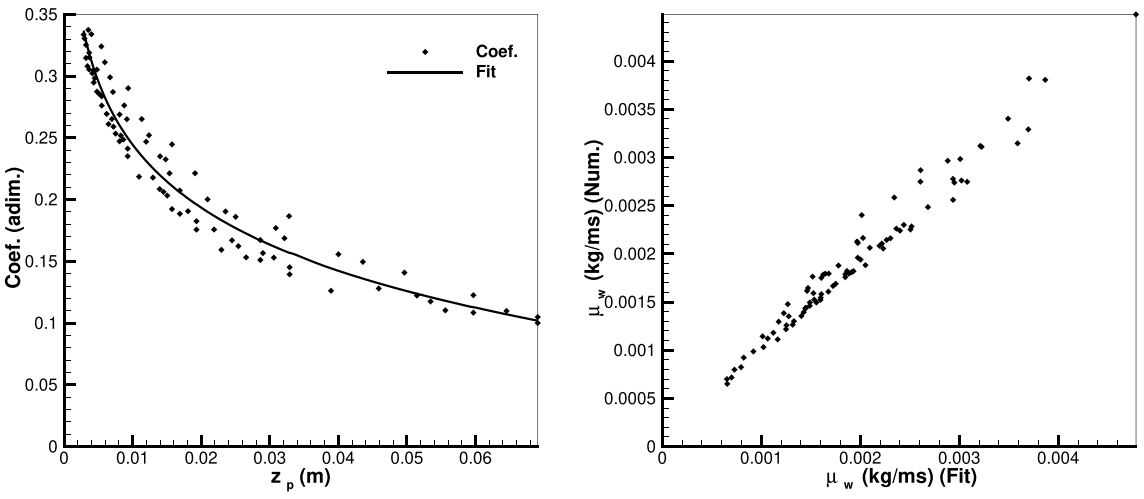

(a) (b)

Fig. 1 **a** Values of coefficient f_μ (from Eq. (63) and **b** Values of μ_w numerical versus μ_w calculated by Eq. (64), using f_μ from Eq. (63)

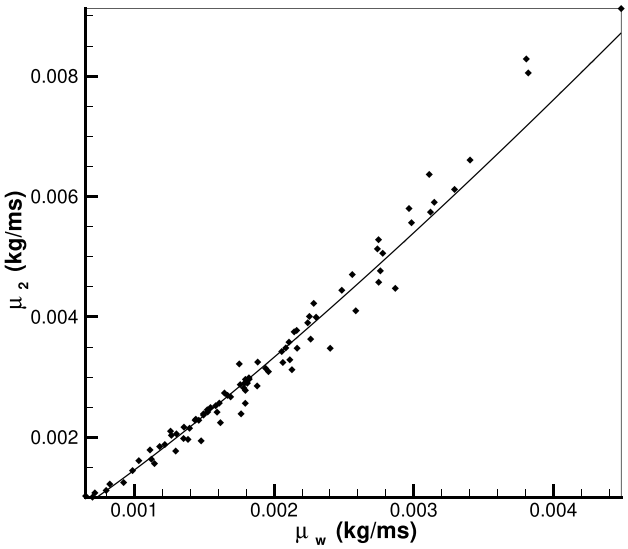

Fig. 2 Values of μ_w versus $\mu_t(z_2)$ and the correspondent fitted equation

1. The simplified $k-\epsilon$ turbulence model is given by Eq. (48) and Eq. (49).
2. The constants are: $c_{\epsilon 1}=0.92$, $c_{\epsilon 2}=1.08$, $c_3=0.00$, $\sigma_\epsilon=1.00$ and $\sigma_k=1.00$.
3. The turbulent viscosity is calculated as a linear function of k, (not k^2) by Eq. (12).
4. The viscosity at the wall is calculated by our adjusted equation, Eq. (66) (with f_μ taken from Eq. (65)).
5. The constant $k^\star$ is calculated using Eq. (59).
6. The boundary conditions at the wall are $\frac{\partial k}{\partial z}=0$ and $\frac{\partial \epsilon}{\partial z}=0$.

4 Application of the simplified $k-\epsilon$ turbulence model to the pollutants dispersion problem

In the Praire Grass experiment, described in [2] the pollutant (SO_2), was continuously released by the source located at $z_s=0.5m$ and measured $1.5m$ above the ground. These measurements were taken in arcs with a radius of 50, 100, 200, 400 and 800m centered in the source. Then, these measurements were integrated in cross wind direction, so that we can reproduce this experiment in two dimensional simulations. The reference velocity are provided at reference position $h_r=10m$. The roughness was determined as $z_0=0.006m$. In order to test the validity of the simplified $k-\epsilon$ turbulence model, it was carried out the computational implementation of this turbulence model coupled with the problem of dispersion of pollutants.

The numerical description of the flow is based on the Reynolds-average Navier-Stokes equations (RANS) for steady conditions. The mathematical model includes the continuity equation

$$\frac{\partial(\rho u)}{\partial x}+\frac{\partial(\rho w)}{\partial z}=0 \tag{67}$$

the momentum equation in axial and vertical directions

Table 2 Meteorological parameters and concentrations measured during the Prairie Grass unstable experiment. Q ($10^{-3}kg/s$) is the emission rate and C_y ($10^{-3}kg/m^2$) is the crosswind integrated concentrations

Exp.	T_g	$u_\star$	λ	–L	z_i	$w_\star$	u_{ref}	Q	C_{50m}	C_{100m}	C_{200m}	C_{400m}	C_{800m}
1	22.5	.166	.0117	9	860	.84	3.2	82	7.00	2.3	.51	.16	.062
5	31.1	.378	.0159	28	780	1.64	7.0	78	3.30	1.80	.81	.29	.092
7	31.2	.266	.0160	10	1340	2.27	5.1	90	4.00	2.20	1.00	.40	.18
8	31.6	.288	.0132	18	1380	1.87	5.4	91	5.10	2.60	1.10	.39	.14
9	27.2	.454	.0128	31	550	1.70	8.4	92	3.70	2.20	1.00	.41	.13
10	30.8	.283	.0162	11	950	2.01	5.4	92	4.50	1.803	.71	.20	.032
16	26.5	.182	.0126	5	1060	2.03	3.6	93	5.00	1.80	.48	.10	.017
19	28.8	.388	.0140	28	650	1.58	7.2	102	4.50	2.20	.86	.27	.058
20	31.0	.619	.0145	62	710	1.92	11.3	102	3.40	1.80	.85	.34	.13
25	24.7	.164	.0115	6	650	1.35	3.2	104	7.90	2.70	.75	.30	.063
26	30.3	.422	.0166	32	900	1.86	7.8	98	3.90	2.20	1.04	.39	.127
27	32.2	.411	.0141	30	1280	2.08	7.6	99	4.30	2.30	1.16	.46	.176
30	34.6	.462	.0147	39	1560	2.23	8.5	98	4.20	2.30	1.11	.40	.10
43	34.5	.324	.0158	16	600	1.66	6.1	99	5.00	2.40	1.09	.37	.12
44	36.8	.387	.0184	25	1450	2.20	7.2	101	4.50	2.30	1.09	.43	.14
49	23.8	.431	.0170	28	550	1.73	8.0	102	4.30	2.40	1.16	.45	.15
50	29.0	.431	.0164	26	750	1.91	8.0	103	4.20	2.30	.91	.39	.11
51	31.0	.435	.0176	40	1880	2.30	8.0	102	4.70	2.40	1.00	.38	.084
61	31.0	.505	.0176	38	450	1.62	9.2	102	3.50	2.10	1.14	.53	.20

$$\frac{\partial(\rho uu)}{\partial x}+\frac{\partial(\rho uw)}{\partial z}=-\frac{\partial p}{\partial x}+\frac{\partial}{\partial x}\left[(\mu+\mu_t)\frac{\partial u}{\partial x}\right]+\frac{\partial}{\partial z}\left[(\mu+\mu_t)\frac{\partial u}{\partial z}\right] \tag{68}$$

$$\frac{\partial(\rho wu)}{\partial x}+\frac{\partial(\rho ww)}{\partial z}=-\frac{\partial p}{\partial x}+\frac{\partial}{\partial x}\left[(\mu+\mu_t)\frac{\partial w}{\partial x}\right]+\frac{\partial}{\partial z}\left[(\mu+\mu_t)\frac{\partial w}{\partial z}\right] \tag{69}$$

where ρ is the air density, taken as constant in this model.

The temperature profile is taken in linear form (T is not unknown)

$$T(z)=T_g-\lambda z \tag{70}$$

where T_g is the ground temperature, and λ is the lapse rate. The values of T_g and λ are taken from Prairie Grass experiment (see Table 2).

As can be seen in Eq. (70), in this work we have not solved the temperature equation. Instead, we simply assume a linear profile, suitable for the mixed layer.

The diffusion equation is

$$\frac{\partial(uC)}{\partial x}+\frac{\partial(wC)}{\partial z}=\frac{\partial}{\partial x}\left[\left(\frac{\mu_t}{\rho S_{c_t}}\right)\frac{\partial C}{\partial x}\right]+\frac{\partial}{\partial z}\left[\left(\frac{\mu_t}{\rho S_{c_t}}\right)\frac{\partial C}{\partial z}\right] \tag{71}$$

where S_{c_t} is the turbulent Schmidt number. In this work, we found that $S_{c_t}=1.25$ is suitable to achieve a good agreement between numerical and experimental data.

In this work, we use our simplified $k-\epsilon$ turbulence model, given by Eq. (48) and Eq. (49). The P_k term, in two-dimensional form, is

$$P_k=\mu_t\left[2\left(\frac{\partial u}{\partial x}\right)^2+2\left(\frac{\partial w}{\partial z}\right)^2+\left(\frac{\partial u}{\partial z}+\frac{\partial w}{\partial x}\right)^2\right] \tag{72}$$

Here, following [12], the term G_k is expressed as

$$G_k=-\beta|g|\frac{\mu_t}{\sigma_T}\left(\frac{\partial\theta}{\partial z}\right)=-\beta|g|\frac{\mu_t}{\sigma_T}\left(\frac{\partial T}{\partial z}+\frac{|g|}{c_p}\right) \tag{73}$$

where $c_p=1.0048\frac{kj}{kgK}$ is the specific heat capacity of air, and $\sigma_T=0.9$ is the turbulent Prandtl number for energy, and β is the thermal expansion coefficient, defined as

$$\beta=-\frac{1}{\rho}\frac{\partial\rho}{\partial T}\approx\frac{1}{T} \tag{74}$$

Using the Finite Volume Method (FVM), with the SIMPLE algorithm and TDMA solver, this mathematical model was solved decoupled of the concentration equation, where firstly the velocity and turbulence fields are achieved, and then the concentration equation is solved. The iterative process are carried out until the mass residuals (for velocity field) becomes less than 10^{-5} and relative error (for k , ϵ and C) becomes less than 10^{-7}. This implementation is robust and stable, so it is possible to obtain high precision.

For all nineteen experiments shown in Table 2, the mesh size in the z direction is calculated based on the length z_i. We find that, for experiment number 7 ($z_i=1340$), a good vertical discretization is found with 500 volumes. Therefore, for other experiments, the mesh size is calculated by direct proportion, that is, $M=\frac{500}{1340}z_i$. In the x direction, the length is 800m for all experiments, and the discretization is always done with 400 volumes. We use a non-uniform mesh in vertical and horizontal directions, with more refinement closer to the pollutant source ($x=0$) and the ground ($z=0$).

4.1 Boundary conditions for *u*, *w*, *C*, k and ϵ

Table 3 presents the boundary conditions for the velocity, concentration, k and ϵ.

The deposition of pollutants on ground surface is taken into account through the deposition flux (F_z), calculated as the product of vertical deposition velocity (v_d) and the ambient concentration near the soil. In this work, we adopt $v_d=0.015$.

For the concentration equation, in the position of emission of the pollutant, the boundary condition is modified for $C=\rho_{SO_2}$, where $\rho_{SO_2}=2.4kg/m^3$. We assume that the pollutant injection velocity is the same of the wind profile, that is, $u(z=0.5m)$. Consequently, the width of the volume where the pollutant is injected (Δy_s) must be adjusted so that the mass flow of the experiment is satisfied, that is, $Q=\rho_{SO_2}u_s\Delta y_s\Delta z_s$, where u_s is the wind velocity at $0.5m$ calculated by the wind profile. The height of the volume where the pollutant is injected (Δz_s) is fixed as 0.04502 m, based on the Praire Grass experiment. As stated, the

Table 3 Boundary conditions for u, w, C, k and ϵ

	u	w	C	k	ϵ
Inlet	$u=\frac{u^*}{\kappa}ln\left(\frac{z+z_0}{z_0}+\psi_m\left(\frac{z}{L}\right)\right)$	$w=0$	$C=\begin{cases}0, & \text{if } z\neq z_s\\ \rho_{SO_2}, & \text{if } z=z_s\end{cases}$	Periodic	Periodic
Outlet	$\frac{\partial u}{\partial x}=0$	$w=0$	$\frac{\partial\overline{C}}{\partial x}=0$	Periodic	Periodic
Ground	$u=0$	$w=0$	$F_z=-v_dC(x,z(2))$	$\frac{\partial k}{\partial z}=0$	$\frac{\partial\epsilon}{\partial z}=0$
Top	$u=\frac{u^*}{\kappa}ln\left(\frac{z_i+z_0}{z_0}+\psi_m\left(\frac{z}{L}\right)\right)$	$w=0$	$\frac{\partial\overline{C}}{\partial x}=0$	$k=0$	$\frac{\partial\epsilon}{\partial z}=0$

numerical simulation was performed in two dimensions (x and z directions). In the y direction, we use only one volume, with width Δy_s, necessary to carry out the cross-wind integration of the numerical pollutants concentration.

4.2 Boundary conditions for $k-\epsilon$

In periodic boundary conditions, the equations relative to the inlet and outlet domain are modified in such a way that the inlet recognizes the outlet as its neighbor and vice versa. In this work, the k and ϵ equations are solved using periodic boundary conditions at both the inlet and outlet positions, in order to ensure a homogeneous solution, so that the outlet profile agrees with the inlet profile. In addition, for faster convergence, we have adopted the following strategy:

1. First, the turbulence model is resolved only in the vertical direction (only one volume is assigned in the axial direction). This is possible due to the imposition of a periodic boundary condition at the inlet and outlet of the flow.
2. After obtaining the vertical profiles of k and ϵ, they are mirrored in the two-dimensional mesh and then the velocity and turbulence equations are resolved in a coupled manner.
3. Finally, having obtained the solutions for u, w, k, ϵ, the concentration equation is solved in an uncoupled manner.

5 Numerical results

The simplified turbulence model presented in this work shows desirable numerical characteristics, such as, robustness, stability and fast convergence. In addition, using periodic boundary conditions together with an adequate viscosity value on the wall, provides a homogeneous solution when applied to the stable and unstable atmospheric boundary layer.

5.1 The effect of the $c_{\epsilon 1}$ and $c_{\epsilon 2}$ constants on the numerical solution

To analyse the effect of the constants $c_{\epsilon 1}$ and $c_{\epsilon 2}$ in the numerical simulation of neutral atmosphere, we take the parameters of experiment number 49 (see Tab. 2), as an example, and remove the buoyancy term (G_k) in Eq. (48) and the term ϕ_m in the velocity profile (Eq. (16)). This fictitious neutral experiment is used to simulate a case of neutral HHTBL. For this case, Fig. 3a shows the numerical solution for k and μ_t. As can be seen, the numerical solutions for k and μ_t are in concordance with the analytical solution, that is $k = u_\star^2$ and $\mu_t = \rho u_\star k(z + z_0)$. For this experiment, $u_\star \approx 0.44$ and $k^\star = k \approx 0.19$.

In Fig. b, we show that changing the values of $c_{\epsilon 1}$ and $c_{\epsilon 2}$ does not significantly modify the numerical solution of μ_t. The only requirement is that $c_{\epsilon 1}$ and $c_{\epsilon 2}$ must satisfy Eq. (57).

5.2 Comparison between the simplified and standard $k-\epsilon$ models for unstable atmosphere

We performed the numerical simulation of experiment number 49 with the standard and simplified $k-\epsilon$ turbulence models, with the same boundary conditions, as shown in Tab. 3. In both cases, the turbulent eddy viscosity at the wall is calculated using the iterative process presented by Eq. (63) and Eq. (64). The numerical solution for velocity and turbulent eddy viscosity are shown in Fig. 4.

As we can see in Fig. 4a, only for the simplified $k-\epsilon$ model the outlet velocity profile remains very close to the

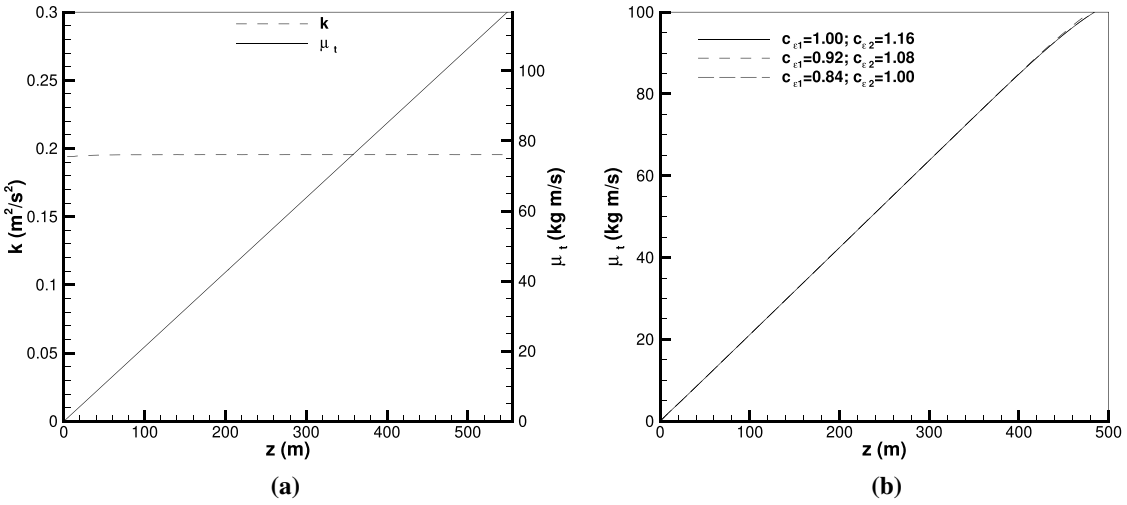

Fig. 3 Profiles of: **a** Numerical solution for k and μ_t. **b** Numerical solution for μ_t for three different combinations of $c_{\epsilon 1}$ and $c_{\epsilon 2}$

inlet profile. As mentioned earlier, this discrepancy in the velocity profiles along the flow is a known deficiency of the standard $k-\epsilon$ model. On the other hand, with the simplified $k-\epsilon$ model, using the iterative process (Eq. (63) and Eq. (64)) or Eq. (66) to calculate μ_w , this requirement is satisfied, even for different meshes. In Fig. 4b, we can see that the behavior of the turbulent eddy viscosity is similar in shape, but distinct in magnitude. As will be shown later, the shape and magnitude of μ_t are directly related to the numerical solution of the dispersion of pollutants. In addition, the magnitude of μ_t obtained with the simplified $k-\epsilon$ model is very close to that obtained using the Troen and Mahrt equation (Eq. 20).

In addition, we choose experiment 49 to investigate the influence of $c_{\epsilon 1}$ and $c_{\epsilon 2}$ on the numerical solution. Figure 5 shows that, by increasing $c_{\epsilon 1}$ (and consequently $c_{\epsilon 2}$, to satisfy Eq. (57)), k and μ_t also increases. However, in the range considered, this variation is negligible.

5.3 Numerical solution of the simplified $k-\epsilon$ turbulence model applied to Praire-Grass experiments

In the following, we will focus our attention on the numerical solution of unstable Praire-Grass experiments with the simplified $k-\epsilon$ turbulence model. Figure 6a and Fig. 6b

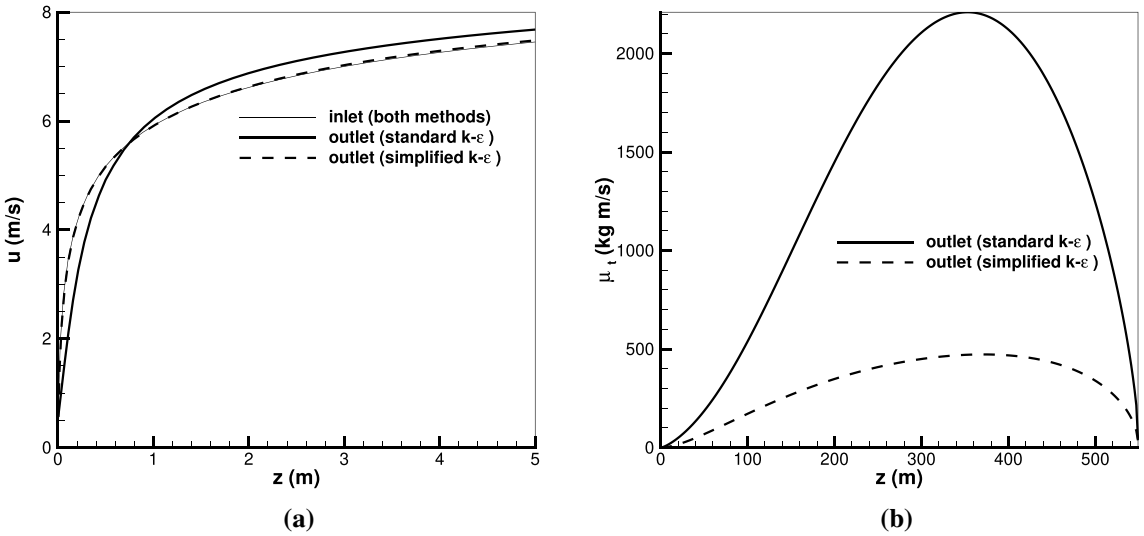

Fig. 4 Profiles of: **a** velocity u (k) and **b** turbulent eddy viscosity (μ_t) concerning experiment number 49

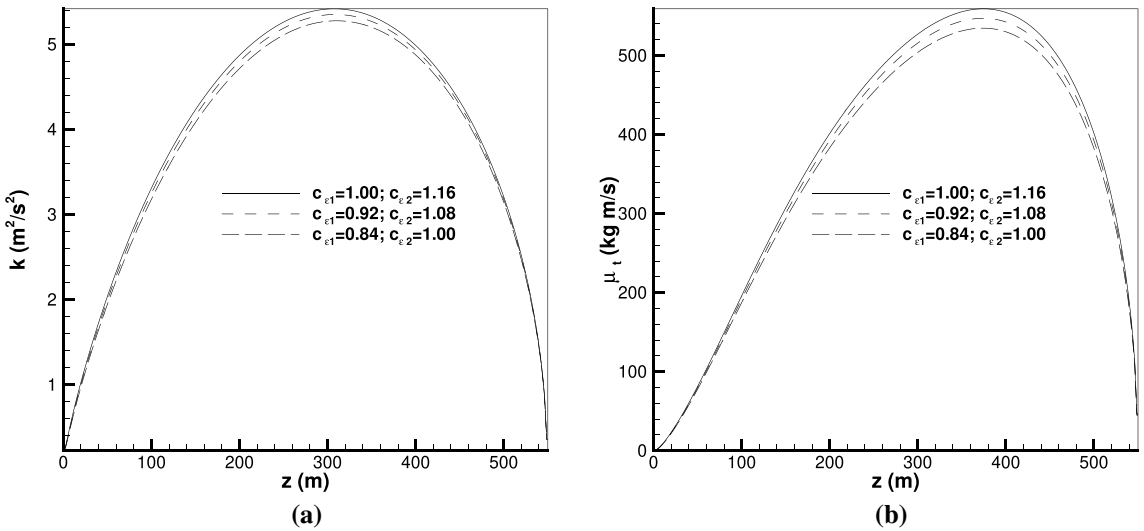

Fig. 5 Effect of changing $c_{\epsilon 1}$ and $c_{\epsilon 2}$ on the (k) profile and **b** Effect of changing $c_{\epsilon 1}$ and $c_{\epsilon 2}$ on the (μ_t) profile

shows the numerical solution of turbulent kinetic energy and turbulent eddy viscosity by contours plot, relative to experiment number 49, as an example.

As can be observed, this solution is horizontally homogeneous, since the contours stay unchanged in horizontal direction, due to the use of periodic boundary conditions.

Extending this analysis, Fig. 7a and Fig. 7b shows the vertical profiles of kinetic energy and turbulent eddy dissipation. These profiles are taken at the middle of the horizontal length, but as can be seen in Fig. 6, they do not change along the horizontal length. The form of the parabolic profile shown in Fig. 7a agrees with the second degree polynomial of Eq. (25). Also, the form of the curve shown in Fig. 7b agrees with the Eq. (23). In Fig. 7b, we limit the display in z to the range $0 \leq z \leq 20$ for clarity.

Figure 8a shows the profile of the turbulent eddy viscosity. The form of these profiles suggest that μ_t changes from linear to parabolic shape, as indicated by Eq. (34) and Eq. (35) due to the fact that the dominant force changes from advection to convection.

Figure 8b shows the inlet and outlet velocity profile. There is no significant difference between these two curves, indicating that, when using the methodology presented in this work, the numerical solution of the velocity field is horizontally homogeneous, as is necessary for this mathematical model.

The profiles for k and ϵ obtained by numerical simulation for all nineteen experiments shown in table 2 were adjusted using the GNU Octave *leasqr* function.

To model the k profile, we chose the equation developed in Sect. 2.6, with one parameter a_1, in the form of

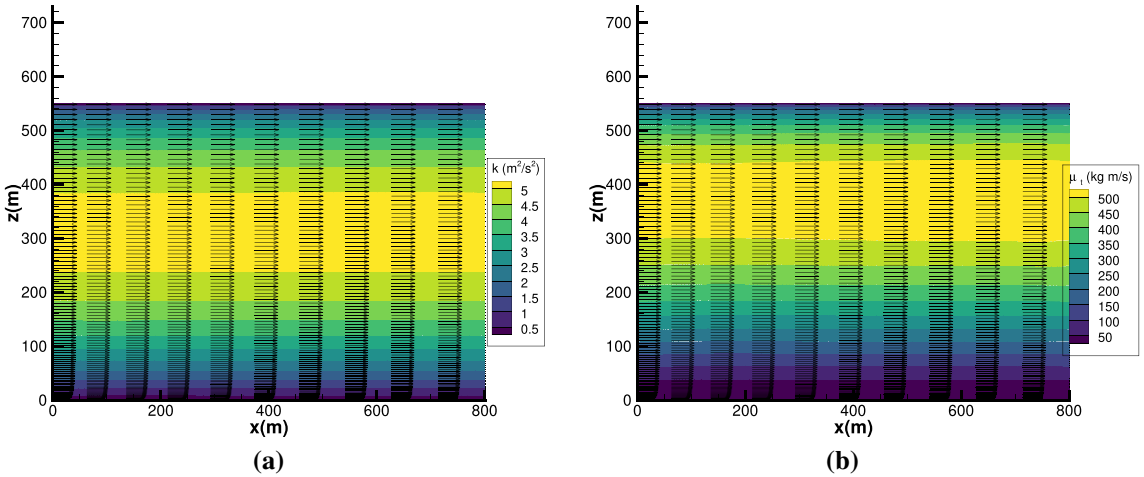

Fig. 6 Contours of: **a** turbulent kinetic energy (k) and **b** turbulent eddy viscosity (μ_t) concerning experiment number 49

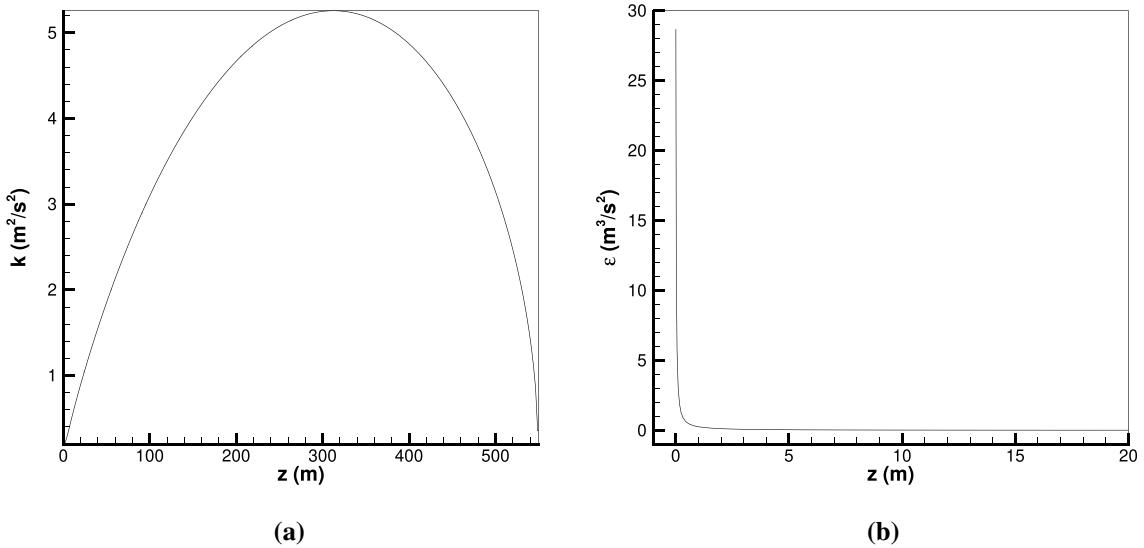

Fig. 7 **a** Profile of turbulent kinetic energy (k) and **b** turbulent eddy dissipation (ϵ), concerning experiment number 49

$$k = a_1 \frac{k^\star}{|L|} z' \left(1 - \frac{z'}{z_i}\right) \tag{75}$$

The fitted parameter was $a_1 = 5.7655$.

To model the ϵ profile, we choose a model like the Eq. (23) with two parameters b_1 and b_2, in the form

$$\epsilon = b_1 \frac{u_\star^3}{\kappa z'} + b_2 \frac{u_\star^3}{\kappa z_i} \tag{76}$$

and the fitted coefficients were $b_1 = 1.3236$ and $b_2 = 2.6654$.

Using Eq. (75) and Eq. (76), the turbulent eddy viscosity can be calculated by Eq. (12), where $k^\star$ is calculated by Eq. (59). To show the agreement between these algebraic equations and the numerical solutions, we chose experiments numbers 49 and 61, as example, to plot numerical versus adjusted profiles. The results are presented in Fig. 9.

For the turbulent kinetic energy, Fig. 9 shows that Eq. (75) provides a good approximation to the numerical solution.

Likewise, for the turbulent eddy dissipation, Fig. 10 shows that Eq. (76) also provides a good approximation to the numerical solution. In this figure, we limit the z and ϵ axis in the range [0 20], for more clarity.

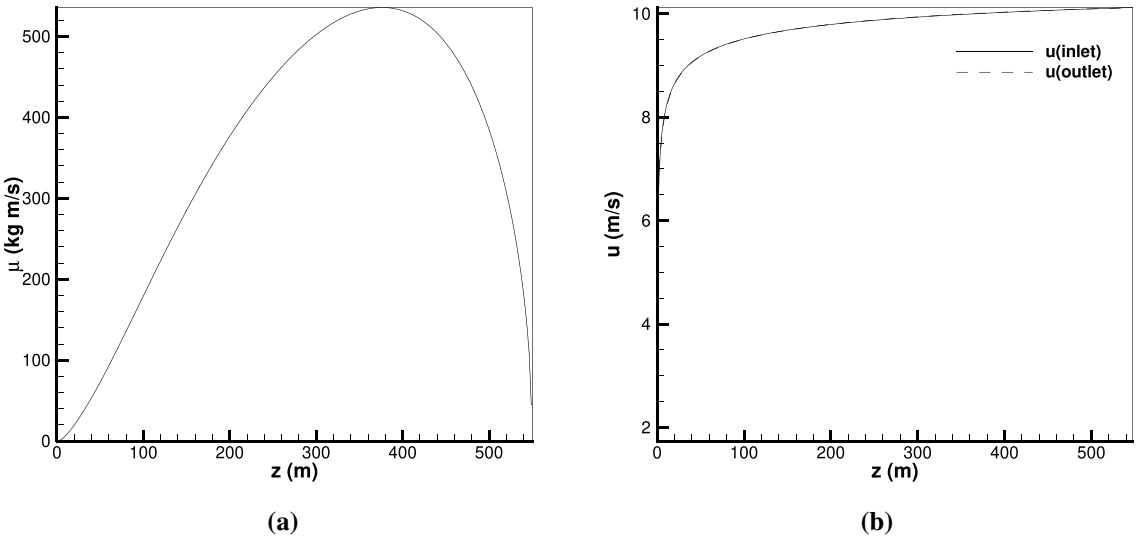

Fig. 8 **a** Profile of turbulent eddy viscosity (μ_t) and **b** profile of inlet and outlet velocity, concerning experiment number 49

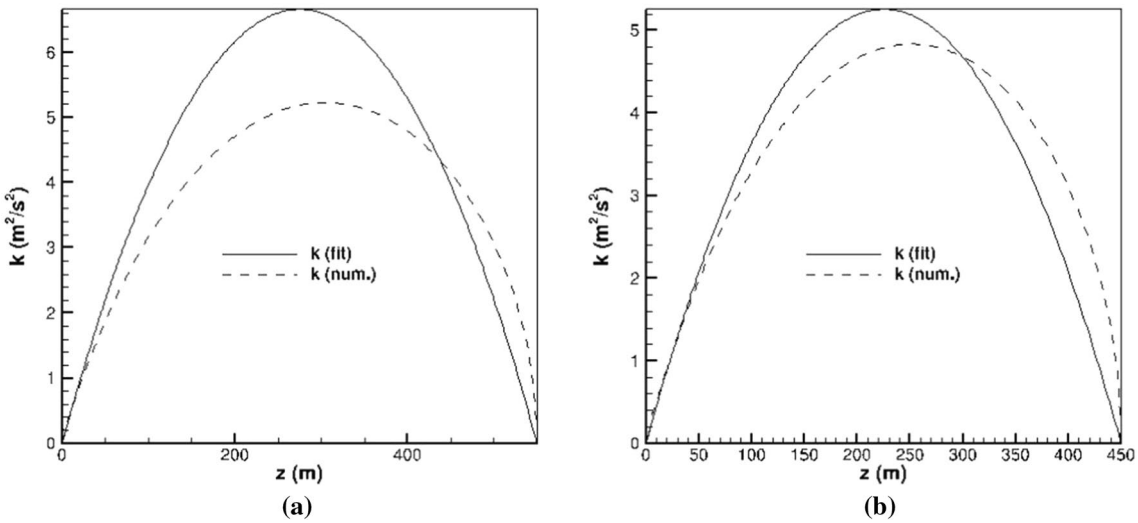

Fig. 9 **a** Turbulent kinetic energy (k) for experiment 49 and **b** for experiment 61

Finally, Fig. 11 shows that equations for k and ϵ can be used to calculate μ_t (using Eq. (12)), providing a good approximation to the numerical solution.

For the other experiments, the comparison between the numerical solution and the equation behaves similarly, but it will not be shown here for the sake of brevity.

5.4 Numerical solution of the concentration equation

The numerical solution of turbulence model provides the turbulent eddy viscosity that is used to calculate the diffusion coefficient $\left(D = \frac{\mu_t}{\rho S_{c_t}}\right)$ that appears in the concentration equation.

In Fig. 12a and b are shown, as examples, the numerical solution of the concentration field for experiments 1 and 20. We chose these experiments because experiments 1 and 20 have a greater difference in their reference velocity (see Table 2).

As can be seen from the figures, in experiment number 1, the concentration spreads more in the vertical direction due to the fact that, for this experiment, the reference velocity (u_{ref} = 3.2 m/s) is lower than that of experiment 20 (u_{ref}=11.3 m/s). Again, we can see that the flow (represented by arrows) is homogeneous,

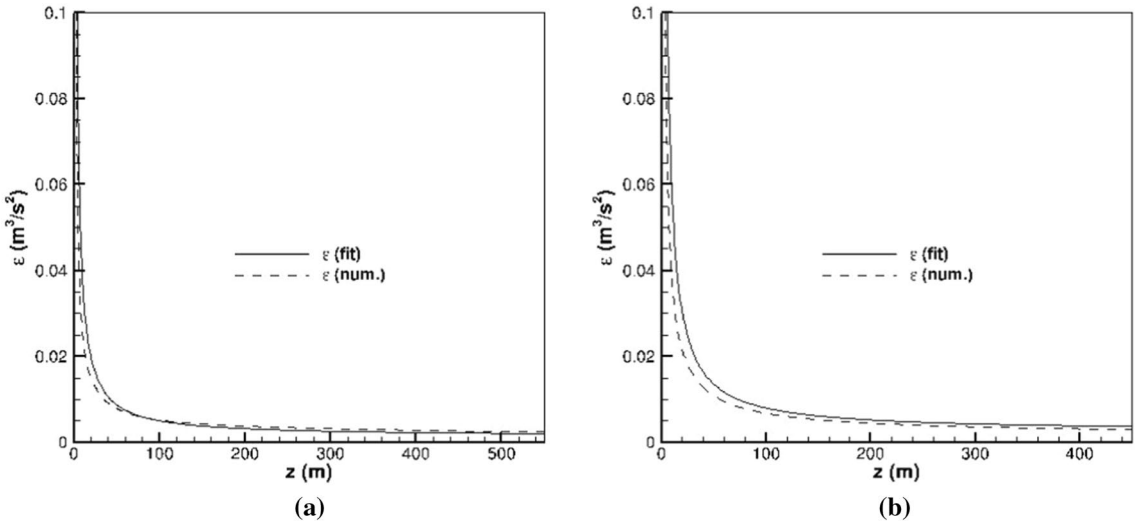

Fig. 10 **a** Turbulent eddy dissipation (ϵ), for experiment 49 and **b** for experiment 61

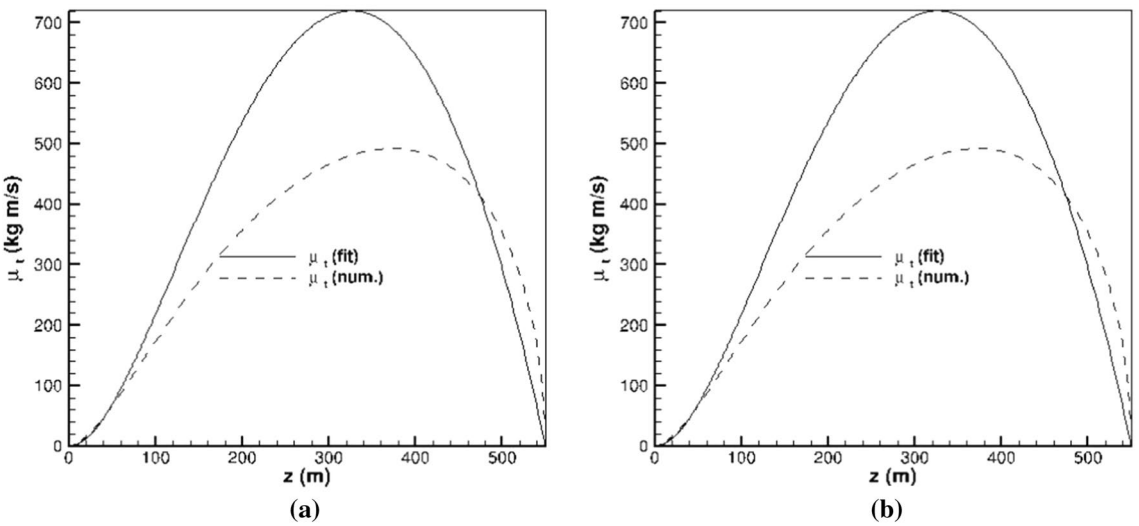

Fig. 11 **a** Turbulent eddy viscosity (μ_t), for experiment 49 and **b** for experiment 61

that is, the velocity profile remains unchanged along the flow direction. The same occurs for the other experiments.

Figure 13 shows the comparison between the numerical solution and the experimental data for the concentration of SO_2 in relation to experiments 1, 20 and Fig. 14 shows these comparisons for experiments 49 and 61.

As can be seen in Figs. 13 and 14, there is a good agreement between these profiles. The same occurs to others experiments listed in Table 2 but they will not be presented here for the sake of brevity.

6 Conclusion

In this paper, we developed a variance of the standard $k-\epsilon$ turbulence model, named simplified $k-\epsilon$ turbulence model. The modifications include a new way to calculate the turbulent eddy viscosity as function of the ratio $\frac{k}{\epsilon}$, an algebraic equation to express the wall viscosity and new values to the constants $c_{\epsilon 1}$, $c_{\epsilon 2}$ and σ_ϵ.

Using periodic boundary conditions to simulate the unstable Praire-Grass experiments, we find horizontally homogeneous numerical solutions for the velocity and turbulence fields. In addiction, we solved the concentration equation and obtained numerical results that agree very well with the experimental data.

We show that this simplified $k-\epsilon$ turbulence model can be used successfully to simulate the atmospheric boundary layer, and we believe that it can be applied to other types of flow.

Moreover, we adjust algebraic equations for k and ϵ profiles that can be used, for example, as initial or boundary conditions in computational codes that do not make use of periodic boundary conditions.

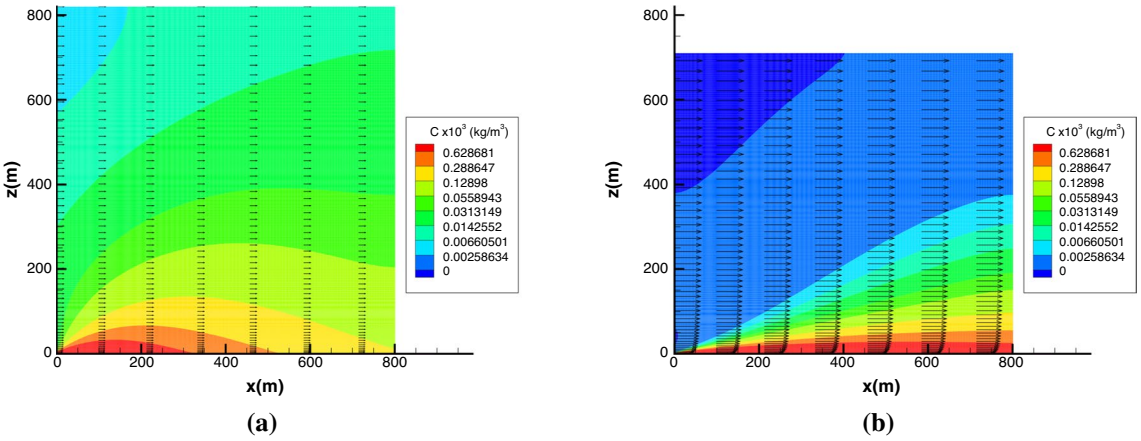

Fig. 12 **a** Concentration field for experiment 1 **b** Concentration field for experiment 20

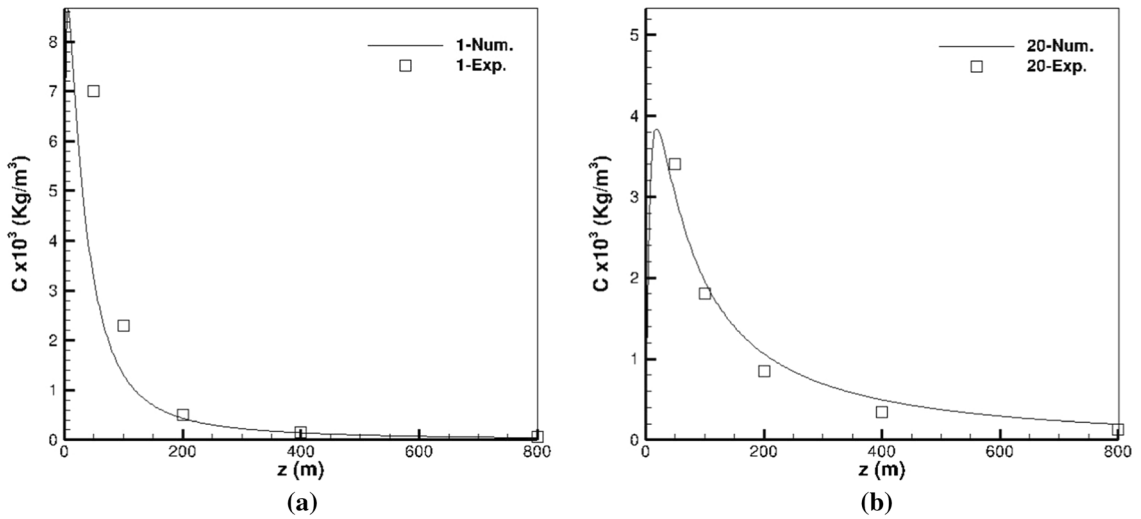

Fig. 13 Comparison of numerical concentration versus experimental data, for experiments **a** 1 and **b** 20

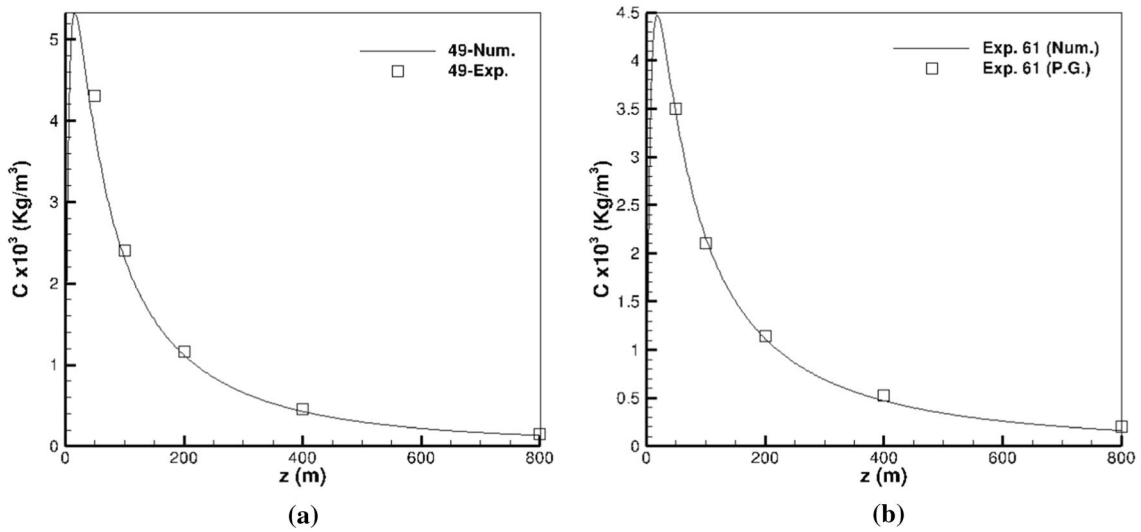

Fig. 14 Comparison of numerical concentration versus experimental data, for experiments **a** 49 and **b** 61

References

1. Alinot C, Masson C (2005) $k-\epsilon$ model for the atmospheric boundary layer under various thermal stratifications. Journal of Solar Energy Engineering-transactions of The Asme - J SOL ENERGY ENG 127. https://doi.org/10.1115/1.2035704
2. Barad, N.: Project Praire Grass: A Field Program in Diffusion, 9 edn. Geophysical Research Papers (1958)
3. Brost RA, Haagenson PL, Kuo YH (1988) The effect of diffusion on tracer puffs simulated by a regional scale eulerian model. Journal of Geophysical Research 93:2389–2404
4. Celik, I.B.: Introductory Turbulence Modeling. Mechanical and Aerospace Engineering Dept, West Virginia University, P.O. Box 6106, Morgantown, WV 26506-6106. (1999)
5. Couvreux F, Bazile E, Canut G, Seity Y, Lothon M, Lohou F, Guichard F, Nilsson E (2016) Boundary layer turbulent processes and mesoscale variability represented by numerical weather prediction models during the bllast campaign. Atmospheric Chemistry Physics 16:8983–9002
6. Degrazia GA, Moreira DM, Vilhena MT (2001) Derivation of an eddy diffusivity depending on source distance for vertically inhomogeneous turbulence in a convective boundary layer. Journal of Applied Meteorology 40:1233–1240
7. Hargreaves DM, Wright NG (2007) On the use of the $k-\epsilon$ model in commercial cfd software to model the neutral atmospheric boundary layer. Journal of Wind Engineering and Industrial Aerodynamics 95:355–369
8. Laan MP, Kelly MC, Sorensen N (2016) A new $k-\epsilon$ model consistent with monin-obukhov similarity theory. Wind Energy 00:1–11
9. Mazzoldi FA, Hill T, Colls JJ (2008) Cfd and gaussian atmospheric dispersion models: A comparation for leak from carbon dioxide transportation and storage facilities. Atmospheric Environment 47:8046–8054
10. Norris, S.E., Richards, P.J.: Appropriate boundary conditions for computational wind engineering models revisited. Fifth Symposium on computational Wind Engineering (2010)
11. Norris, S.E., Richards, P.J.: Appropriate boundary conditions for a pressure driven boundary layer. 18 th Australasian Fluid Mechanics Conference (2012)
12. Pieterse JE, Harms TM (2013) Cfd investigation of the atmospheric boundary layer under different thermal stability conditions. Journal of Wind Engineering and Industrial Aerodynamics 121:82–97
13. Pleim JE, Chang JS (1992) A non-local closure model for vertical mixing in the convective boundary layer. Atmospheric Environment 26A:965–981
14. Pontiggia M, Derudi M, Alba M, Scaioni M (2010) Hazardous gas releases in urban areas: Assessment of consequences through cfd modelling. Hazardous Materials 176:589–596
15. Pope, S.B.: Turbulent flows. Cambridge Univ. Press, Cambridge (2011). https://cds.cern.ch/record/1346971
16. Richards PJ, Hoxey RP (2010) Appropriate boundary conditions for computational wind engineering models using the $k-\epsilon$ turbulence model. Journal of Wind engineering and Industrial Aerodynamics 46:145–153
17. Sundqvist H, Veronis G (1970) A simple finite-difference grid with non-constant intervals. Tellus 22(1):26–31. https://doi.org/10.3402/tellusa.v22i1.10155
18. Troen IB, Mahrt L (1986) A simple model of the atmospheric boundary layer: Sensitivity to surface evaporation. Boundary-Layer Meteorology 37:129–148